Astronomy
&
Astrophysics

The Ital-FLAMES survey of the Sagittarius dwarf spheroidal galaxy

I. Chemical abundances of bright RGB stars[⋆,⋆⋆]

L. Monaco[1,2], M. Bellazzini[2], P. Bonifacio[1], F. R. Ferraro[3],
G. Marconi[4], E. Pancino[2], L. Sbordone[5,6], and S. Zaggia[1]

[1] Istituto Nazionale di Astrofisica – Osservatorio Astronomico di Trieste, via Tiepolo 11, 34131 Trieste, Italy
  e-mail: lmonaco@eso.org
[2] Istituto Nazionale di Astrofisica – Osservatorio Astronomico di Bologna, 40127 Bologna, Italy
[3] Università di Bologna – Dipartimento di Astronomia, 40127 Bologna, Italy
[4] European Southern Observatory, Casilla 19001, Santiago, Chile
[5] Istituto Nazionale di Astrofisica – Osservatorio Astronomico di Roma, via Frascati 33, 00040 Monteporzio Catone,
  Roma, Italy
[6] Università Tor Vergata, Roma, Italy

Received 28 April 2005 / Accepted 22 June 2005

Abstract. We present iron and α element (Mg, Ca, Ti) abundances for a sample of 15 Red Giant Branch stars belonging to the main body of the Sagittarius dwarf Spheroidal galaxy. Abundances have been obtained from spectra collected using the high resolution spectrograph FLAMES-UVES mounted at the VLT. Stars of our sample have a mean metallicity of [Fe/H] = -0.41 ± 0.20 with a metal-poor tail extending to [Fe/H] = -1.52. The α element abundance ratios are slightly subsolar for metallicities higher than [Fe/H] $\gtrsim -1$, suggesting a slow star formation rate. The [α/Fe] of stars having [Fe/H] < -1 are compatible to what observed in Milky Way stars of comparable metallicity.

Key words. stars: atmospheres – Galaxy: abundances – galaxies: evolution – galaxies: dwarf – galaxies: individual: Sgr dSph

1. Introduction

The Local Group (LG) is a heterogeneous environment. Galaxies in the LG show a variety of characteristics (e.g. mass, morphology, gas content) and are evolving under different conditions (e.g. in isolation, on strong dynamical interaction). Thererore, in principle, they could teach us about galaxy evolution as much as globular clusters did concerning stellar evolution. Chemical abundances and abundance ratios are key ingredients to study the star formation histories of stellar systems. The modern generation of spectrographs mounted on 8–10 m class telescopes allows us to investigate the chemical composition and dynamics of bright stars in LG galaxies but only a handful of stars have been studied so far (Tolstoy et al. 2004, 2003; Shetrone et al. 2003; Bonifacio et al. 2000, 2004; Fulbright et al. 2004; Geisler et al. 2005; Shetrone et al. 1998, 2001).

The commonly accepted paradigm (White & Rees 1978) predicts the formation of large galaxies from the hierarchical assembly of small fragments similar to the LG dwarf spheroidals (dSphs). In this framework, the comparison between the chemical composition of the Milky Way (MW) and LG dSph stars is a first local testbed for the hierarchical merging model. The chemical composition of LG stars turned out to be remarkably different from that of MW stars of comparable metallicities. In particular, LG stars show α element abundance ratios systematically under-abundant with respect to MW stars (see, for instance, Venn et al. 2004; Bonifacio et al. 2004). The interpretation of this empirical evidence is controversial. Is the hierarchical merging a minor process in the assembly of the MW? Or were the fragments from which the MW formed at early times different from the nowadays recognizable dSphs? The chemical difference between MW and LG stars may reflect an environmental difference between dwarfs accreted at early times (galaxies near the bottom of the pre-MW potential well – dense environment) and the surviving dwarfs (galaxies far from the bottom of the pre-MW potential well – loose environment, but see Robertson et al. 2005; Bullock & Johnston 2004).

[⋆] Based on observations obtained with FLAMES at VLT Kueyen 8.2 m telescope in the program 71.B-0146.
[⋆⋆] Appendix A is only available in electronic form at
http://www.edpsciences.org

The Sagittarius dSph (hereafter Sgr, Ibata et al. 1994) is a LG galaxy currently experiencing strong and disruptive tidal interactions with the MW (Ibata et al. 1995, 1997; Majewski et al. 2003). Therefore, it may provide clues on the influence of dynamical interactions on the chemical evolution of dwarf galaxies.

It is well-known that the complex stellar content of Sgr (see Monaco et al. 2002; Monaco et al. 2003, 2005, and references therein) is largely dominated by a population of old-intermediate age stars (~6 Gyr, see, e.g. Bellazzini et al. 1999; Layden & Sarajedini 2000; Monaco et al. 2002). However, some concerns have been raised on mean metallicity estimates obtained for this population from spectroscopic and photometric works (see, e.g. Mateo et al. 1995; Bonifacio et al. 2000; Cole 2001; Monaco et al. 2002; Bonifacio et al. 2004).

The paper is devoted to the assessment of the mean chemical properties of the Sgr dominant population. We present Fe, Mg, Ca and Ti abundances for a selected sample of stars belonging to this population. In a companion paper (Bonifacio et al., in preparation) we deal with the issue of the Sgr metallicity distribution.

[Fe/H] and [α/Fe] abundances as well as the trends in the [Fe/H] vs. [α/Fe] plane constrain the chemical evolution which led to the formation of the Sgr dominant population (Lanfranchi & Matteucci 2003). Moreover, mean [Fe/H] and [α/Fe] values are key ingredients to derive reliable age estimates from the color−magnitude diagrams.

The paper is organized as follows. In Sect. 2 we describe the target selection and the obtained data. In Sect. 3 we describe the procedures followed to fix the atmospheric parameters and the chemical analysis. In Sect. 4 we compare the results obtained with previous works and in Sect. 5 we discuss our findings.

2. Observations

2.1. Target selection, data and equivalent widths

As part of the guaranteed time awarded to the Ital-FLAMES consortium, more than 400 stars were observed in the Sgr dSph (Bonifacio et al. 2005; Zaggia et al. 2004) from May the 23th to 27th, 2003, using the FLAMES facility mounted on the VLT (Pasquini et al. 2000). Details on the observations are given in Zaggia et al. (2004). FLAMES allows us to observe 132 targets in one shot using the intermediate-low resolution spectrograph GIRAFFE, plus 8 additional targets using the red arm of the high resolution specrograph UVES. In this paper we present the results obtained from the UVES spectra.

It is important to recall that a large number of Milky Way foreground stars are present along the Sgr line of sight. In order to optimize the Sgr star detection rate, the target selection for the UVES fibres was performed using the infrared 2 MASS[1] color magnitude diagram (CMD). In fact, in the infrared plane, the upper Sgr red giant branch (RGB) stands out very clearly from the contaminating MW field (see, e.g., Cole 2001). This also allows a thorough sampling of the Sgr dominant population. In Fig. 1 we plotted the 2 MASS (K; $J − K_{\rm S}$) CMD for
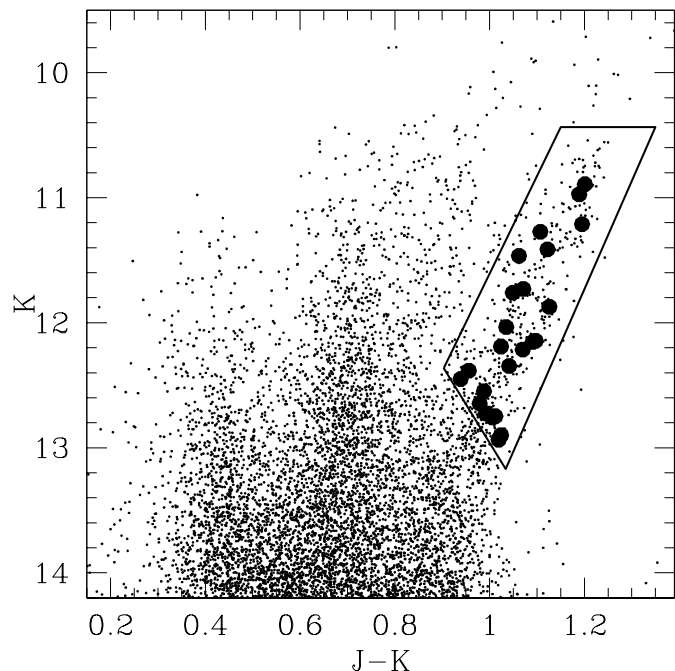

Fig. 1. The K vs. $J − K_{\rm S}$ 2 MASS color–magnitude diagram for a one square degree region around the globular cluster M 54. Target stars are plotted as large filled circles.

a 1 square degree area centred on the globular cluster M 54. The heavy continuous line is the selection box. Target stars are plotted as large filled circles. A similar target selection already proved to be very effective in detecting stars belonging to the Sgr Stream (Majewski et al. 2004).

Target stars are marked as large symbols in the optical CMD plotted in Fig. 2 (Monaco et al. 2002). In Table 1 we report equatorial (J 2000.0) coordinates and V and I magnitudes for the target stars.

The coordinates in the J2000.0 absolute astrometric system for both UVES and GIRAFFE samples were obtained with a procedure already described in other papers (see, for example, Ferraro et al. 2001). The new astrometric Guide Star Catalogue (GSC II) recently released and now available on the web[2] was used as reference. In order to derive an astrometric solution we used a program specifically developed at Bologna Observatory (Montegriffo et al., in preparation). As a result of the entire procedure, rms residuals of ~0.15 arcsec, both in RA and Dec, were obtained. The quality of the astrometry was confirmed by the successful centering of the fibres.

We performed the analysis on the spectra reduced with the UVES ESO-MIDAS[3] pipeline. For each pointing, 7 fibres were centred on the target stars while one fibre was used to measure the sky spectrum. Different spectra of the same star were coadded and the resulting signal to noise ratio (*S/N*) ranges from 14 to 43 at 653 nm (see Table 2). UVES spectra have a

---

[1] See http://www.ipac.caltech.edu/2mass

[2] See http://www-gsss.stsci.edu/gsc/gsc2/GSC2home.htm

[3] ESO-MIDAS is the acronym for the European Southern Observatory Munich Image Data Analysis System which is developed and maintained by the European Southern Observatory. http://www.eso.org/projects/esomidas/
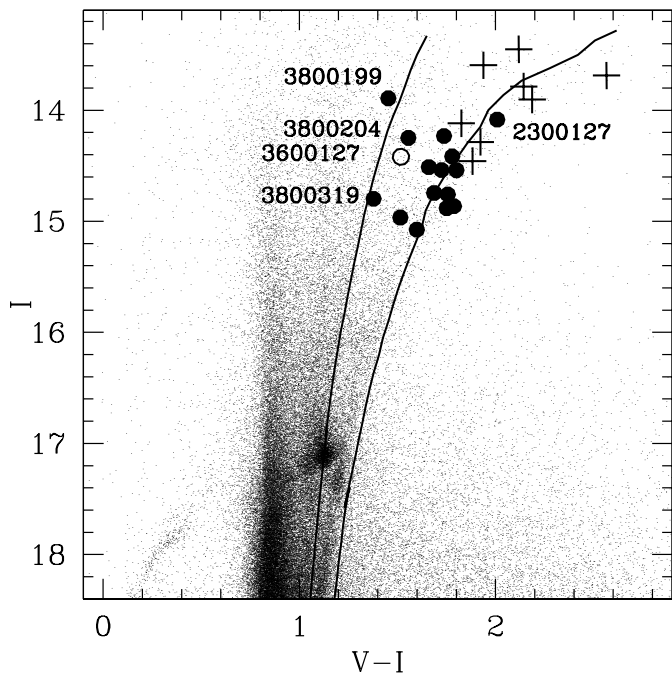
Fig. 2. I vs. $V - I$ color–magnitude diagram for a one square degree region around the globular cluster M 54. Target stars are marked with large symbols. Stars showing TiO molecular bands in the spectra are plotted as plus symbols. Star 3600217 has a radial velocity not compatible with the membership to Sgr and is plotted as a large empty circle. Theoretical isochrones from which the surface gravities for the programme stars were obtained are also plotted as continuous lines.

resolution of $R \simeq 43\,000$ and cover the range between 480 nm and 680 nm.

Equivalent widths (*EW*) were measured on the spectra using the standard IRAF[4] task *splot*. The Fe, Ca, Mg and Ti line lists as well as the adopted atomic parameters and the measured *EW* are reported in Table A.1. A different iron line list (see Table A.2) was adopted for star #3800319 due to the relatively high temperature and gravity of this star in comparison with the other stars in the sample. We analysed interactively the spectral lines. For each line the fit has been visually inspected and adjusted until reaching a satisfying solution.

2.2. Radial velocities and the contaminating Milky Way field

Radial velocities (see Table 1) were obtained by cross-correlating the observed spectra with a rest frame laboratory line list using the recently released software DAOSPEC[5] (Stetson and Pancino, in preparation). The final radial velocities and relative errors were computed using about 150 lines for each star. Geocentric observed radial velocities were corrected to heliocentric velocities using the IRAF task *rvcorrect*.

---

[4] IRAF is distributed by the National Optical Astronomy Observatories, which is operated by the association of Universities for Research in Astronomy, Inc., under contract with the National Science Foundation.

[5] See http://cadcwww.hia.nrc.ca/stetson/daospec

The DAOSPEC code has the capability to measure the line *EW*s. In our case, however, we used DAOSPEC only to measure the radial velocities of the target stars while we used the IRAF task *splot* to measure EWs for homogeneity with our previous works on Sgr stars (Bonifacio et al. 2000, 2004). As a check, the radial velocities of a few stars have also been measured using the *fxcor* IRAF task for Fourier cross correlation. The radial velocities obtained using DAOSPEC and *fxcor* are identical, within the errors.

All but one (#3600127, $v_{\text{helio}} = -127.6$ km s^{-1}, open circle in Fig. 2) of the 24 observed stars are indeed Sgr radial velocity members lying within $\sim 2\sigma$ of the systemic velocity as measured by Ibata et al. (1997). In Fig. 3 we plotted the velocity distribution of the 23 Sgr radial velocity members. The mean velocity ($\langle v_r \rangle = 143.08 \pm 3.2$ km s^{-1})[6] and the velocity dispersion of the sample ($\sigma = 11.17$ km s^{-1}) are in good agreement with the values derived by Ibata et al. (1995) and Ibata et al. (1997).

The MW model of Robin et al. (2003, hereafter R03) predicts that in the M 54 line of sight 2% of stars have $v_r > 100$ km s^{-1}, if we consider only stars lying in the same $(V, V - K)$[7] selection box of the UVES sample. However, the model predicts only a $\sim 4\%$ of giant stars (log $g < 4$) in the selection box and none of them with $v_r > 100$ km s^{-1}. We checked carefully the 24 stars in the sample and we are confident that all of them are indeed red giant. Therefore, even if the R03 model provides only an approximate description of the MW, there is no reason to expect any MW star among the 23 Sgr radial velocity members in the sample.

2.3. M-giants showing TiO molecular bands in the spectra

The coolest (i.e. the reddest) four stars (#2300168, #3600181, #3700055, #4207391, plus symbols at $V - I > 2.0$ in Fig. 2) have effective temperatures around 3600 K and very strong titanium oxide bands (TiO, see Selvelli & Bonifacio 2000; Valenti et al. 1998) in the spectra (see Fig. 4). The presence of the TiO bands confirm these stars as M-giants. Such strong molecular bands prevent from a safe derivation of the equivalent widths. Therefore, we do not present the chemical analysis for these stars. In addition, stars #3600073, #3700178, #3800366, #4207953 (plus symbols at $V - I < 2.0$ in Fig. 2) show weak but clearly recognizable TiO bands. For these stars we provide only a tentative analysis and the derived abundances will not be discussed. We plan to provide a detailed chemical analysis for these 8 stars by performing spectral synthesis including also the TiO molecular bands.

In the CMD in Fig. 2 star #2300127 lies exactly in the region occupied by stars with TiO bands in their spectra. Yet this star does not present any band. The lack of the TiO molecular bands may be due to the relatively weak Fe and Ti content of this star ([Fe/H] = −0.81, [Ti/Fe] = −0.17, see Table 3).

---

[6] The quoted 3.2 km s^{-1} error has been estimated employing a bootstrap technique.

[7] The R03 model does not provide the $(J - K)$ color, therefore we define as selection box in the $(V, V - K)$ plane the region which encloses all the target stars.

Table 1. Coordinates and atmospheric parameters for the program stars.

Star	α (J2000.0)	δ (J2000.0)	V	I	$(V-I)$	$v_{\text{helio}}(\text{km s}^{-1})$	T_{eff}[a]	$\log g$	ξ	[M/H]
2300127	18 55 46.703	−30 35 24.683	16.09	14.08	2.01	+147.2 ± 0.58	3687	0.72	2.0	−1.0
2300196	18 55 30.778	−30 28 19.635	16.26	14.54	1.72	+148.0 ± 0.94	3908	0.97	2.3	−0.5
2300215	18 55 19.146	−30 30 27.978	16.52	14.76	1.76	+154.9 ± 0.79	3877	1.08	1.9	−0.5
2409744	18 54 55.854	−30 32 43.106	16.34	14.54	1.80	+131.7 ± 0.80	3837	0.97	1.8	−0.5
3600230	18 53 45.818	−30 25 49.419	16.43	14.74	1.69	+153.8 ± 0.56	3947	1.08	1.6	−0.5
3600262	18 53 22.340	−30 23 47.172	16.63	14.88	1.75	+156.0 ± 0.61	3882	1.16	1.9	−0.5
3600302	18 53 45.209	−30 30 55.702	16.65	14.86	1.79	+143.8 ± 0.67	3848	1.15	1.6	−0.5
3800199	18 55 13.453	−30 26 42.249	15.35	13.90	1.45	+138.8 ± 0.63	4245	0.72	1.9	−1.0
3800204	18 55 5.7440	−30 27 56.602	15.81	14.25	1.56	+153.2 ± 0.61	4101	0.93	2.4	−1.5
3800318	18 54 58.264	−30 28 20.165	16.20	14.42	1.78	+151.8 ± 0.84	3856	0.90	1.9	−0.5
3800319	18 54 58.088	−30 28 58.481	16.18	14.80	1.38	+141.1 ± 0.88	4364	1.23	1.9	−1.5
4303773	18 54 02.120	−30 36 21.665	15.97	14.23	1.74	+143.1 ± 0.63	3895	0.80	1.9	−0.5
4304445	18 53 40.606	−30 35 42.879	16.17	14.51	1.66	+119.9 ± 0.59	3976	0.95	1.7	−0.5
4402285	18 53 19.765	−30 37 40.099	16.48	14.97	1.51	+159.2 ± 0.61	4156	1.20	1.5	−0.5
4408968	18 53 12.886	−30 32 03.565	16.67	15.07	1.60	+144.0 ± 0.68	4047	1.26	2.0	−0.5
3600073⋆	18 53 56.477	−30 27 20.337	15.53	13.59	1.94	+156.2 ± 0.67	3731	0.41	2.0	−0.5
3700178⋆	18 54 18.068	−30 29 31.259	16.34	14.46	1.88	+149.1 ± 0.81	3770	0.92	2.3	−0.5
3800336⋆	18 55 11.635	−30 28 00.544	16.21	14.29	1.92	+131.1 ± 0.74	3741	0.83	2.0	−0.5
4207953⋆	18 54 14.546	−30 32 34.502	15.94	14.11	1.83	+129.0 ± 0.89	3815	0.74	1.9	−0.5
2300168⋆	18 55 20.010	−30 26 45.824	16.25	13.68	2.57	+136.0 ± 2.81	3599			
3600181⋆	18 53 57.440	−30 25 09.207	16.09	13.90	2.19	+147.3 ± 1.23	3610			
3700055⋆	18 54 2.6250	−30 26 48.807	15.57	13.45	2.12	+121.9 ± 1.34	3634			
4207391⋆	18 54 24.849	−30 33 02.291	15.93	13.79	2.14	+133.7 ± 2.01	3624			
3600127	18 53 22.441	−30 23 59.172	15.94	14.42	1.52	−127.6 ± 0.51	4152			

[a] We adopted a reddening of $E(V-I) = 0.18$.
⋆ Star showing TiO molecular bands in the spectra.

3. Atmospheric parameters and chemical analysis

The UVES spectra of the 19 stars for which the chemical analysis was performed (including also stars having weak TiO bands) are plotted in Fig. 5.

3.1. Effective temperatures and surface gravities

The effective temperatures for the target stars (see Table 1) were derived from the $(V-I)$ color assuming a reddening of $E(V-I) = 0.18$ (Layden & Sarajedini 2000) and using the calibration of Alonso et al. (1999).

We used the Girardi et al. (2002) theoretical isochrones, along with $E(V-I) = 0.18$ and $(m-M)_0 = 17.10$ (Layden & Sarajedini 2000; Monaco et al. 2004) as reddening[8] and

distance modulus, in order to estimate the gravity of the program stars. In particular, we used a ($Z = 0.001$; Age = 14.13 Gyr) isochrone for stars #3800199 #3800204 #3800319 and a ($Z = 0.008$; Age = 6.31 Gyr) isochrone for all the other stars (continuous lines in Fig. 2). These two isochrones fit into the range covered by the target stars on the CMD and the age and metallicity used are also compatible to what expected from previous works (see Monaco et al. 2002; Layden & Sarajedini 2000; Brown et al. 1999; Bonifacio et al. 2004).

3.2. Model atmosphere and microturbulent velocities

For each star we computed a plane parallel model atmosphere using version 9 of the ATLAS code (Kurucz 1993) with the above atmospheric parameters. Abundances were derived from EWs using the WIDTH code (Kurucz 1993).

Microturbulent velocities (ξ) were determined minimizing the dependence of the iron abundance from the EW, among the set of iron lines measured for each star.

Table 2. Mean chemical abundances for the program stars. The signal to noise ratio of the coadded spectra and the number of lines used are also reported.

Star[a]	S/N @653 nm	A(Fe)	n	A(Mg)	n	A(Ca)	n	A(Ti)	n
Sun		7.51		7.58		6.35		4.94	
2300127	20	6.70 ± 0.24	15	6.82 ± 0.15	2	5.35 ± 0.10	9	3.99 ± 0.06	7
2300196	20	7.02 ± 0.19	15	7.03 ± 0.18	4	5.67 ± 0.16	9	4.49 ± 0.16	9
2300215	14	7.28 ± 0.18	13	7.04 ± 0.18	4	5.98 ± 0.22	9	4.84 ± 0.25	9
2409744	22	7.25 ± 0.06	10	7.09 ± 0.03	2	5.82 ± 0.08	8	4.67 ± 0.13	9
3600230	21	7.34 ± 0.18	16	7.24 ± 0.17	4	5.81 ± 0.14	9	4.63 ± 0.14	9
3600262	21	7.14 ± 0.18	15	7.27 ± 0.13	3	5.58 ± 0.19	9	4.34 ± 0.18	9
3600302	24	7.20 ± 0.18	15	7.03 ± 0.14	4	5.85 ± 0.11	9	4.53 ± 0.17	9
3800199	32	6.41 ± 0.17	15	6.52 ± 0.08	4	5.60 ± 0.10	8	4.32 ± 0.11	8
3800204	31	5.99 ± 0.08	13	6.28 ± 0.04	2	4.97 ± 0.07	5	3.65 ± 0.10	8
3800318	23	6.98 ± 0.17	16	6.83 ± 0.15	4	5.88 ± 0.18	9	4.69 ± 0.17	9
3800319	21	6.14 ± 0.26	32	6.56 ± 0.09	2	5.38 ± 0.15	7	4.14 ± 0.14	7
4303773	18	6.78 ± 0.15	14	6.66 ± 0.16	4	5.47 ± 0.17	9	3.98 ± 0.05	7
4304445	33	7.16 ± 0.14	16	7.21 ± 0.05	2	5.76 ± 0.21	9	4.45 ± 0.13	9
4402285	22	7.22 ± 0.13	15	7.11 ± 0.17	4	5.99 ± 0.25	9	4.79 ± 0.13	9
4408968	18	7.09 ± 0.16	17	6.81 ± 0.04	3	5.82 ± 0.11	9	4.56 ± 0.12	9
3600073★	43	6.73 ± 0.18	17	6.67 ± 0.14	4	5.23 ± 0.15	9	3.87 ± 0.20	9
3700178★	19	7.06 ± 0.19	16	6.83 ± 0.17	3	5.47 ± 0.32	9	4.16 ± 0.24	9
3800336★	25	6.88 ± 0.16	14	7.01 ± 0.10	3	5.63 ± 0.12	8	4.40 ± 0.16	9
4207953★	30	7.10 ± 0.13	15	6.97 ± 0.10	4	5.63 ± 0.19	9	4.51 ± 0.17	8

★ Star showing TiO molecular bands in the spectra.
$A(X) = \log\left(\frac{X}{H}\right) + 12.00$.
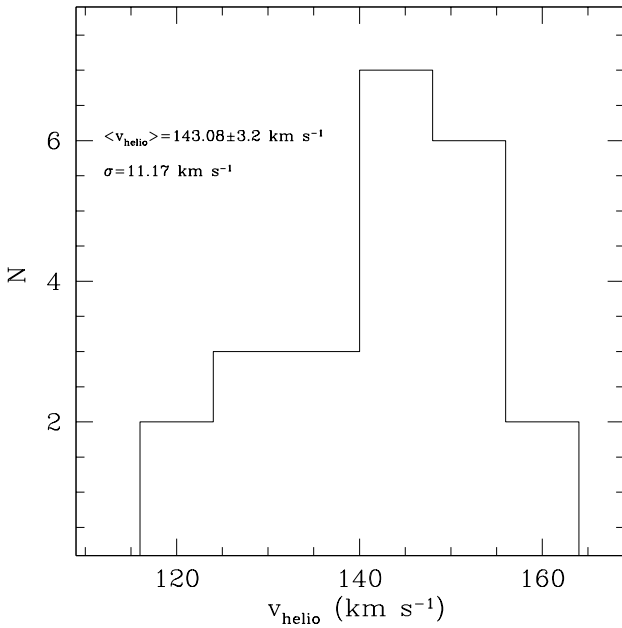
Fig. 3. Heliocentric radial velocity distribution for the 23 programme stars Sgr radial velocity members.

In Fig. 6 we plotted ξ as a function of the adopted gravity for the stars studied by Ivans et al. (2001, bottom panel, hereafter I01), Shetrone et al. (2003, middle panel, hereafter S03) and for stars in our sample (top panel). A clear trend is present in both the I01 and S03 samples. The same trend is present also in our sample, albeit with a larger scatter. Continuous lines are least square fits to the data points. In the case of our sample the fit was obtained excluding the points having the highest and lowest ξ (2.7 and 0.6 km s^{-1}) and the point with the lowest surface gravity (log g = 0.41). As can be seen, the three fitting lines are very similar to each other. A weak dependence of the ξ from the effective temperature was found and it can be safely neglected as a first order approximation. For stars #2300127, #2300215 and #3800319 (filled circles in Fig. 6) the ξ is 2.7, 2.5 and 0.6 km s^{-1}, respectively, i.e. more than 2-σ far from the fitting relation. When working with low S/N, highly crowded spectra, it is difficult to measure weak Fe lines accurately. This may lead to incorrect ξ. Thus, for stars #2300127, #2300215 and #3800319 we adopted the value obtained from the fitting relation $\xi = -0.35 \times \log g + 2.29$, i.e. ξ = 2.0, 1.9 and 1.9 km s^{-1}, respectively.
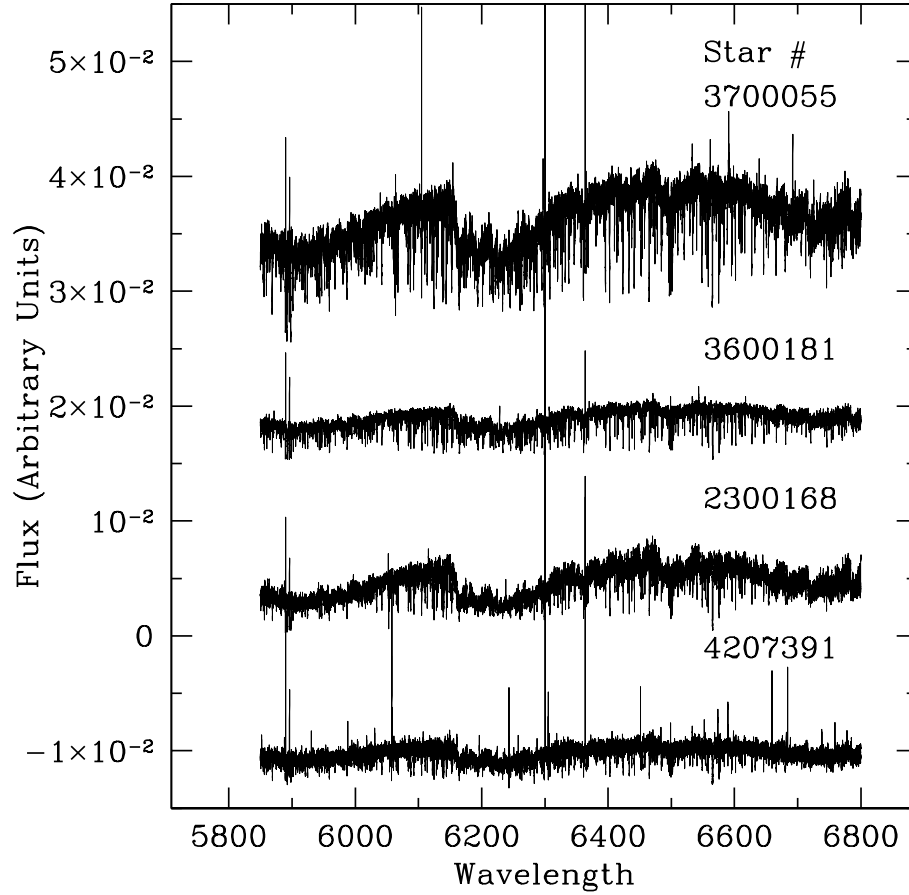
Fig. 4. Coadded UVES spectra of the 4 Sgr M-giants having strong TiO bands.

3.3. Chemical abundances

The atmospheric parameters (T_{eff}, $\log g$, ξ and the assumed global metallicity [M/H]) adopted for the program stars are reported in Table 1. The chemical abundances obtained for each line are reported in Tables A.1 and A.2. The mean and standard deviation of such abundances are reported in Tables 2 and 3 (as [X/H] abundances in the latter case) for each chemical species. In Table 2 we also reported the number of lines used to obtain the mean abundance for each species. The line scatter reported in Table 2 should be representative of the statistical error arising from the noise in the spectra and from uncertainties in the measurement of the equivalent widths.

Under the assumption that each line provides an independent measure of the abundance, the error in the mean abundances should be obtained by dividing the line scatter by $\sqrt{n}$ (where n is the number of measured lines) and by adding to this figure the errors arising from the uncertainties in the atmospheric parameters. In Table 4 we report these latter errors in the case of star #3800318, taken as representative of the whole sample.

In Fig. 7 we plotted the metallicity distribution obtained. Our sample spans a rather large metallicity range ($-1.52 \leq$ [Fe/H] ≤ -0.17). The distribution peaks around [Fe/H] $\simeq -0.4$

and presents an extended metal poor tail[9]. In particular, considering only stars more metal rich than [Fe/H] $\simeq -1$, which should be representative of the Sgr dominant population, we obtain a mean value of $\langle$[Fe/H]$\rangle = -0.41 \pm 0.20$.

In Fig. 8 we plotted the [Ti/Fe], [Ca/Fe] and [Mg/Fe] ratios (from top to bottom panel) for the program stars as a function of the [Fe/H] abundance. The 5 M 54 stars studied by Brown et al. (1999, hereafter B99) are plotted as large open stars. Assuming $\langle[\alpha/\text{Fe}]\rangle = \frac{\text{[Mg/Fe]+[Ca/Fe]}}{2}$, we also obtain a mean value of $\langle[\alpha/\text{Fe}]\rangle = -0.17 \pm 0.07$ for the dominant population.

Following Salaris et al. (1993), these values correspond to a global metallicity[10] of [M/H] $= -0.51$, which is in good agreement with the recent photometric estimate by Monaco et al. (2002).

3.4. Notes on metal poor stars: #3800199, #3800204, #3800319

The three most metal-poor stars (#3800199 #3800204 and #3800319) occupy in the optical CMD (see Fig. 2)

---

[9] Preliminary results obtained from the GIRAFFE sample show that such tail extends at least down to [Fe/H] < -2.5 (Zaggia et al. 2004; Bonifacio et al. 2005).

[10] The "global metallicity" is defined as: [M/H] $=$ [Fe/H] $+ \log (0.638 \times 10^{[\alpha/\text{Fe}]} + 0.362)$.
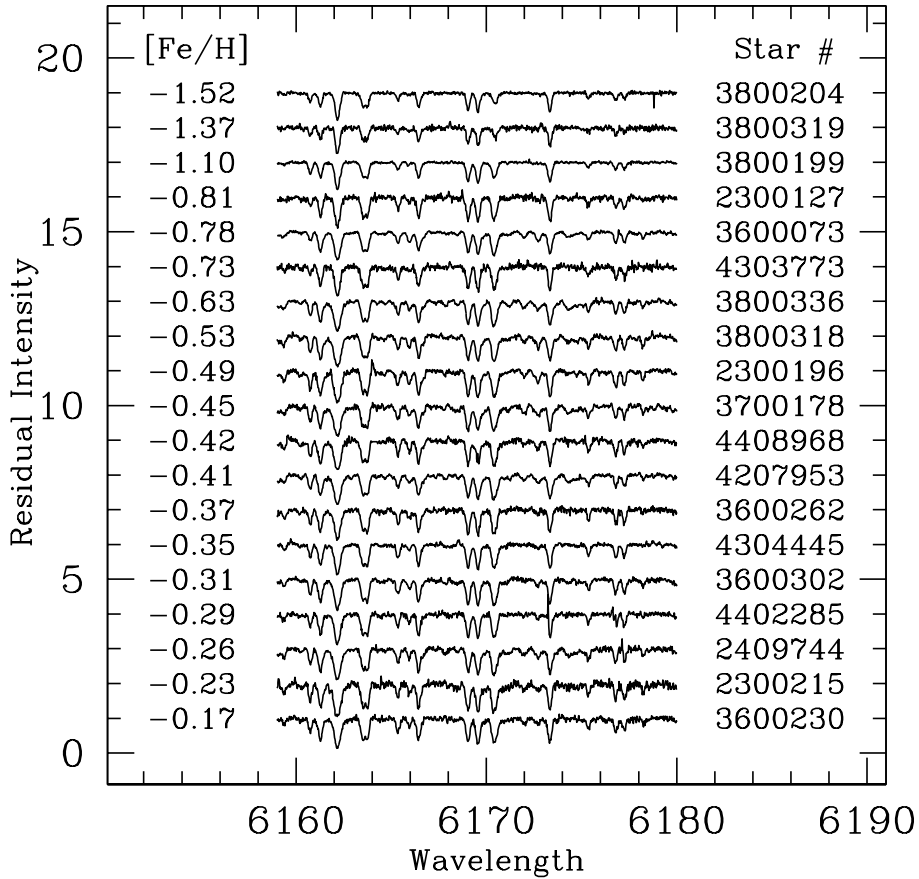
Fig. 5. Coadded UVES spectra of the 19 Sgr giants analyzed in this paper. Labels on the right denote the star number, those on the left the [Fe/H].
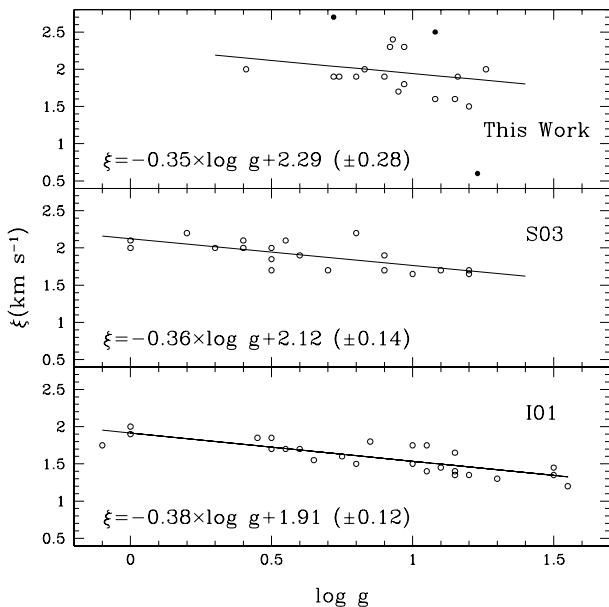

Fig. 6. Microturbulent velocities as a function of the surface gravity for the programme stars (*top panel*) and stars in the S03 and I01 samples (*middle and bottom panel respectively*). Least square fits to the data are plotted as continuous lines. The filled circles in the upper panel mark stars more than 2-σ far from the fitting relation.

positions compatible with the M 54 RGB (which is roughly represented by the bluer isochrone in the plot).

The most metal-poor star (#3800204, [Fe/H] = −1.52) lies very near to the M 54 center (∼1′) and its chemical abundances (Fig. 8) are identical to those of the M 54 stars studied by B99. Therefore, it seems quite likely that this star does indeed belong to M 54.

Star #3800319 ([Fe/H] = −1.37) is also quite near (∼1.′4) to the cluster center but its chemical composition is only marginally compatible with M 54 and it will be considered a Sgr field star. However, we note that Layden & Sarajedini (2000) claimed a metallicity dispersion of ∼0.16 dex for M 54 from the width of the red giant branch.

Star #3800199 ([Fe/H] = −1.10) is placed at 3.′2 from the cluster center (which corresponds to ∼7 half light radii, Trager et al. 1995) and is significantly more metal rich than M 54 ([Fe/H] ∼ −1.55, B99). Therefore, we consider star #3800199 part of the Sgr galaxy field.

4. Comparison with previous works

Beside the present work, chemical abundances have been presented for Sgr RGB stars by Bonifacio et al. (2000, 2004, 2 and 10 stars, respectively) and by Smecker-Hane & McWilliam (2002, hereafter S02, 14 stars). Bonifacio et al. (2004, hereafter B04) also considered the two stars studied in Bonifacio et al. (2000) obtaining a final sample of 12 stars.

In Fig. 9 we plotted the [α/Fe] as a function of the iron abundance for the stars in the 3 samples. Stars in our sample are

Table 3. Mean abundance ratios for the program star.

Star	[Fe/H]	[Mg/Fe]	[Ca/Fe]	[Ti/Fe]
2300127	-0.81 ± 0.24	$+0.05$	-0.19	-0.14
2300196	-0.49 ± 0.19	-0.06	-0.19	$+0.04$
2300215	-0.23 ± 0.18	-0.31	-0.14	$+0.13$
2409744	-0.26 ± 0.06	-0.23	-0.27	-0.01
3600230	-0.17 ± 0.18	-0.17	-0.37	-0.14
3600262	-0.37 ± 0.18	$+0.06$	-0.40	-0.23
3600302	-0.31 ± 0.18	-0.24	-0.19	-0.10
3800199	-1.10 ± 0.17	$+0.04$	$+0.35$	$+0.48$
3800204	-1.52 ± 0.08	$+0.22$	$+0.14$	$+0.23$
3800318	-0.53 ± 0.17	-0.22	$+0.06$	$+0.28$
3800319	-1.37 ± 0.26	$+0.35$	$+0.40$	$+0.57$
4303773	-0.73 ± 0.15	-0.19	-0.15	-0.23
4304445	-0.35 ± 0.14	-0.02	-0.24	-0.14
4402285	-0.29 ± 0.13	-0.18	-0.07	$+0.14$
4408968	-0.42 ± 0.16	-0.35	-0.11	$+0.04$
3600073*	-0.78 ± 0.18	-0.13	-0.34	-0.29
3700178*	-0.45 ± 0.19	-0.30	-0.43	-0.33
3800336*	-0.63 ± 0.16	$+0.06$	-0.09	$+0.09$
4207953*	-0.41 ± 0.13	-0.20	-0.31	-0.02

* Star showing TiO molecular bands in the spectra $[X/Y] = \log\left(\frac{X}{Y}\right) - \log\left(\frac{X}{Y}\right)_\odot$.

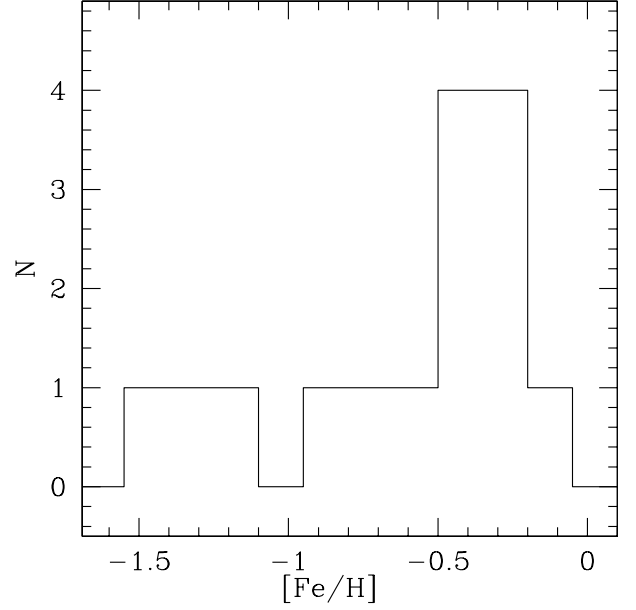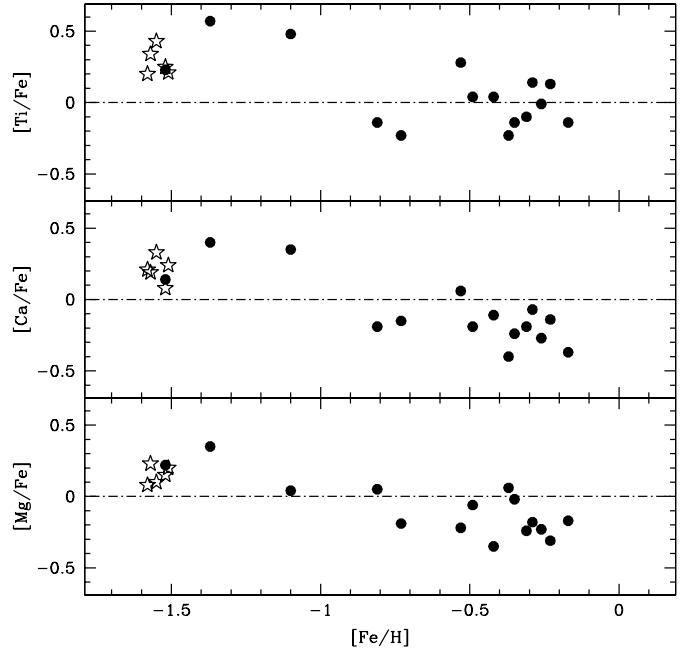**Table 4.** Errors in the abundances of star # 3800318 due to uncertainties in the atmospheric parameters.

	ΔA(Fe)	ΔA(Mg)	ΔA(Ca)	ΔA(Ti)
$\Delta\xi = \pm 0.2$ km s^{-1}	$^{-0.08}_{+0.10}$	∓ 0.04	∓ 0.12	$^{-0.15}_{+0.17}$
$\Delta T_{\rm eff} = \pm 100$ K	$^{-0.04}_{+0.07}$	$^{-0.02}_{+0.05}$	± 0.10	$^{+0.13}_{-0.12}$
$\Delta\log g = \pm 0.50$	$^{+0.16}_{-0.14}$	$^{+0.08}_{-0.07}$	$^{-0.04}_{+0.01}$	± 0.05

Fig. 7. Metallicity distribution of the program stars.

Fig. 8. α element abundance ratios ([Ti/Fe], [Ca/Fe] and [Mg/Fe] *from top to bottom panel*) as a function of the iron abundance for the program stars. Large open stars mark the 5 M 54 stars studied by B99.

plotted as filled circles, while stars in the B04 and S02 sample are plotted as empty squares and empty triangles, respectively. The 5 M 54 stars studied by B99 are marked as large open stars. The α element abundance ratio is defined as $[\alpha/\text{Fe}] = \frac{[\text{Mg/Fe}]+[\text{Ca/Fe}]}{2}$ for stars in our sample and in the B04 and B99 samples, while it is defined as $[\alpha/\text{Fe}] = \frac{[\text{Si/Fe}]+[\text{Ca/Fe}]+[\text{Ti/Fe}]}{3}$ for stars in the S02 sample[11].

Stars in the S02 sample range from [Fe/H] $\simeq -1.6$ to [Fe/H] $\simeq 0$. In particular, 3 stars in their sample have [Fe/H] < -1 and 11 stars are in the range $-0.7 \div 0.0$. This latter subsample has a mean metallicity and α element abundance ratio of: $\langle[\text{Fe/H}]\rangle = -0.36 \pm 0.19$ and $\langle[\alpha/\text{Fe}]\rangle = +0.01 \pm 0.04$. However, it is important to note that these values should not be considered as representative of the dominant population, since

their target selection has been biased toward stars with metallicities within 0.5 dex of the solar value based on previously obtained approximate metallicities (McWilliam & Smecker-Hane 2004).

The metallicity range of stars in the B04 sample, on the other hand, is $-0.83 \leq [\text{Fe/H}] < +0.09$. Therefore, it extends toward slightly higher metallicity with respect to the S02 sample, but it lacks of metal-poor stars. The mean metallicity and α element abundance ratio of the B04 sample are: $\langle[\text{Fe/H}]\rangle = -0.23 \pm 0.26$ and $\langle[\alpha/\text{Fe}]\rangle = -0.20 \pm 0.06$.

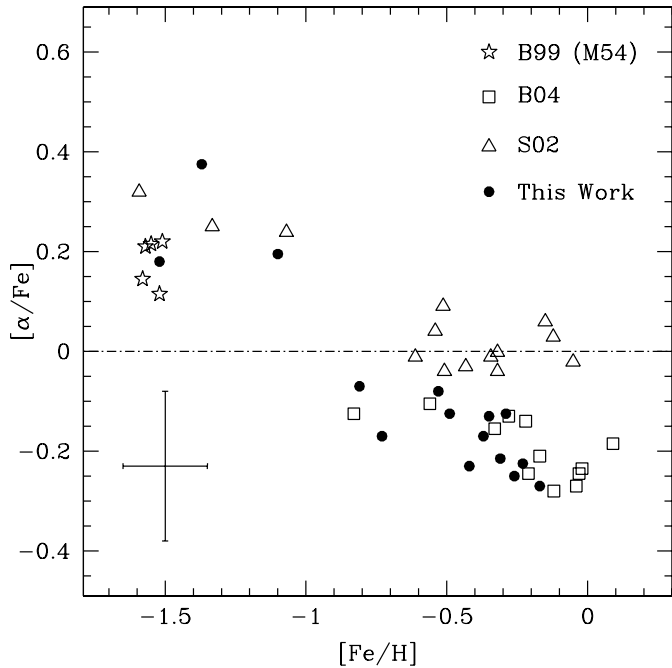[11] S02 do not provide abundances for each species but only mean values.

Fig. 9. α element abundance ratio – defined as: $[\alpha/\text{Fe}] = \frac{[\text{Mg/Fe}]+[\text{Ca/Fe}]}{2}$ – as a function of the iron abundance for the program stars (filled circles). Large open stars mark the 5 M 54 stars studied by B99. Open squares and open triangles mark stars in the B04 and S02 samples, respectively. For stars in the S02 sample: $[\alpha/\text{Fe}] = \frac{[\text{Si/Fe}]+[\text{Ca/Fe}]+[\text{Ti/Fe}]}{3}$.

The mean iron abundance obtained in this paper ([Fe/H] = −0.41) is similar to that of the S02 and B04 samples. The 0.18 dex difference between the B04 mean iron abundance and our figure would be also a little bit lowered (by 0.06 ÷ 0.09 dex) by taking into account the different assumption about the reddening (B04 adopted $E(V - I) = 0.22$ from Marconi et al. 1998). The different target selection criterion adopted by B04 may also be responsible for the residual difference in the mean iron abundance (∼0.1 dex), which is, nevertheless, well inside the involved errors.

The $\langle[\alpha/\text{Fe}]\rangle$ ratio obtained by B04 is very similar to our value ($\langle[\alpha/\text{Fe}]\rangle = \frac{[\text{Mg/Fe}]+[\text{Ca/Fe}]}{2} = -0.17$). S02 evaluate the α element abundance ratio as $[\alpha/\text{Fe}] = \frac{[\text{Si/Fe}]+[\text{Ca/Fe}]+[\text{Ti/Fe}]}{3}$. Considering $[\alpha/\text{Fe}] = \frac{[\text{Ca/Fe}]+[\text{Ti/Fe}]}{2}$, we obtain a $\langle[\alpha/\text{Fe}]\rangle$ fairly similar to the S02 figure. The small residual difference (∼0.1 dex higher in the S02 sample) may be partly ascribed to the [Si/Fe] abundances and, possibly, to a different set of lines and atomic parameters adopted in the chemical analysis. Unfortunately, S02 neither provide abundances for each species nor the atomic data and the adopted line list and this hypothesis cannot be checked further.

Finally, as already stressed in Sect. 3.4, we remark that the Fe, Mg, Ca and Ti abundances of star #3800204 are consistent with the results obtained by B99 for M 54 stars.

5. Discussion and conclusions

The main purpose of this paper was to study the chemical composition of the dominant population of the Sgr dSph galaxy. We selected 24 target stars using the 2 MASS infrared CMD, where the upper RGB of Sgr is well separated from the MW field.

Target stars have been observed using the red arm of the high resolution spectrograph FLAMES-UVES. We reported radial velocities for these 24 stars and all but one are Sgr radial velocity members. Eight stars show strong or visible TiO bands. For stars with weak TiO bands we present a tentative chemical analysis while we do not present any chemical analysis for stars presenting strong TiO bands in the spectra.

For the remaining 15 stars, we reported Fe, Mg, Ca and Ti chemical abundances. This is the largest sample of high resolution spectra analyzed so far for stars in the Sgr dSph galaxy, and the only sample thoroughly representative of the Sgr dominant population.

The metallicity ranges from [Fe/H] = −1.52 to [Fe/H] = −0.17. Three stars have [Fe/H] < −1 and the most metal poor of them (#3800204) can be reasonably considered M 54 member.

The mean iron content of stars with [Fe/H] > −1 (i.e. the Sgr dominant population) is $\langle[\text{Fe/H}]\rangle = -0.41 \pm 0.20$, with a mean α element abundance ratio $\langle[\alpha/\text{Fe}]\rangle = -0.17 \pm 0.07$. These figures lead to a global metallicity [M/H] = −0.51 which is in close agreement with the most recent photometric estimates obtained for the Sgr dominant population (Monaco et al. 2002).

In order to obtain a more statistically significant sample, we now join the B04 and our samples. In Fig. 10 we plotted in the [α/Fe] vs. [Fe/H] plane the mean points obtained for Sgr from this larger sample of Sgr stars as filled circles. For −0.65 < [Fe/H] < 0.1, filled circles represent running means with 0.20 dex as bin and 0.1 dex as step. For stars having −1.0 < [Fe/H] < −0.65 and −1.5 < [Fe/H] < −1 (i.e. excluding star #3800204 which has been tagged as M 54 member) filled circles are straight means of the [Fe/H] and [α/Fe] with the corresponding standard deviations as errorbars. A weak, but clearly recognizable trend between the α element abundance ratio and the mean iron abundance exists at high metallicity. Such a trend waits to be confirmed from a much more extended sample such as that obtained using the FLAMES-GIRAFFE multifibre spectrograph which is currently under analysis. For [Fe/H] < −1, a sudden increase of the [α/Fe] is apparent.

The mean [α/Fe] at low metallicities is consistent with the values observed in MW stars (crosses in Fig. 10, from Venn et al. 2004) of comparable metallicities and somewhat higher with respect to stars in the LG galaxies (asterisks in the figure, from Venn et al. 2004). Therefore, metal-poor stars lost in early passages which now are not recognizable as Sgr tidal debris (Helmi 2004), would be part of the typical content of the MW Halo and impossible to tag as an accreted component from the chemical composition.

The three metal-poor stars in the S02 sample are compatible with MW stars as well. This occurrence led the authors to suggest that the upper mass end of the Sgr initial mass function (IMF) should not be significantly different from the MW one. The level of [α/Fe] which characterizes a galaxy at low metallicities may indeed give information on the IMF of the galaxy at that time (see McWilliam 1997, and references therein), since the amount of α elements and iron produced by a type II SN is a function of the mass of the SN progenitor. Although this is true in principle, in practice this information may not be presently
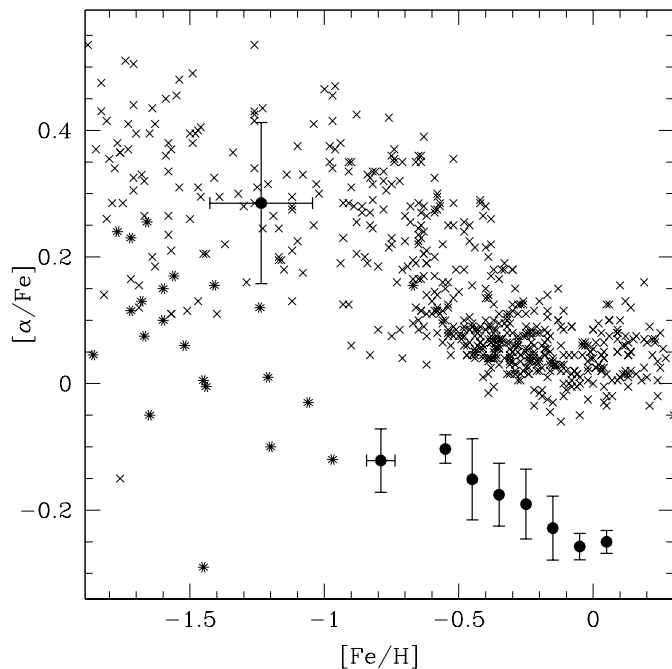
Fig. 10. $[\alpha/\text{Fe}] = \frac{[\text{Mg/Fe}]+[\text{Ca/Fe}]}{2}$ as a function of [Fe/H] for stars in the MW and in Local Group dwarf galaxies (crosses and asterisks, respectively, from Venn et al. 2004). Filled circles are mean points for Sgr obtained joining the B04 sample and our data.

(see, for instance, Kravtsov et al. 2004; Mayer et al. 2001; Zaritsky & Harris 2004).

Finally, we note that the Large Magellanic Cloud (LMC) metallicity distribution strongly resembles the Sgr one. In fact, Cole et al. (2005) approximated the metallicity distribution of the LMC bar by two Gaussians having [Fe/H] = −0.37 ± 0.15 and [Fe/H] = −1.08 ± 0.46 and containing 89% and 11% of the stars, respectively. The same results hold also for the LMC disk (see Cole et al. 2005). Clearly, Sgr has the same mean metallicity of the LMC dominant population as well as the same fraction of metal-poor stars (see Monaco et al. 2003). Such occurrence may suggest a similarity of the Sgr progenitor with the LMC.

extracted. In fact the ratio of the α elements and iron produced by a type II SN is also a sensitive function of the "mass cut", i.e. the mass coordinate which separates the material of the SN which "falls back" on the SN remnant from the material which is ejected. The deeper the mass cut, the more iron-peak elements are ejected, thus lowering the overall $[\alpha/\text{Fe}]$. Current SN models are unable to determine the mass cut in a self consistent way or from first principles: the mass cut is always *assumed*. We do not have either any indication on whether the mass cut is in any sense "Universal" or if it may vary e.g. depending on the mass of the star or on its metallicity. With this state of affairs, any inference on the IMF from the level of the $[\alpha/\text{Fe}]$ ratio of a galaxy would be highly uncertain.

The metal-rich Sgr stars lie on the extension to high metallicity of the pattern followed by stars in LG galaxies and below MW stars. A low $[\alpha/\text{Fe}]$ at high metallicity is traditionally interpreted as evidence for a slow or bursting star formation rate (S02, B04, Marconi et al. 1994). On the contrary, in order to reproduce the Sgr $[\alpha/\text{Fe}]$ ratios, Lanfranchi & Matteucci (2003) required a high star formation rate. However, they constrained their model using preliminary abundances presented by Smecker-Hane & McWilliam (1999). The somewhat lower $[\alpha/\text{Fe}]$ values obtained here and in S02 and B04 should be in better agreement with a lower star formation rate.

Our data suggest that Sgr had a different chemical evolution from both the MW and the LG galaxies (see Fig. 10). A different chemical evolution for Sgr with respect to the other LG galaxies is expected, since Sgr experienced strong and disruptive dynamical interactions with the MW. Such interactions are witnessed by the Sgr tidal tails studied by Majewski et al. (2003) and are expected to trigger star formation activity

References

Alonso, A., Arribas, S., & Martínez-Roger, C. 1999, A&AS, 140, 261
Bellazzini, M., Ferraro, F. R., & Buonanno, R. 1999b, MNRAS, 307, 619
Bonifacio, P., et al. 2004, Proc. of the ESO/Arcetri Conference on Chemical Abundances and Mixing in Stars in the Milky Way and its Satellites held in Castiglione della Pescaia, Italy, 13−17 September
Bonifacio, P., Hill, V., Molaro, P., et al. 2000, A&A, 359, 663
Bonifacio, P., Sbordone, L., Marconi, G., Pasquini, L., & Hill, V. 2004, A&A, 414, 503
Brown, J. A., Wallerstein, G., & Gonzalez, G. 1999, AJ, 118, 1245
Bullock, J. S., & Johnston, K. V. 2004, Proc. of the conference Satellites and Tidal Streams, held in La Palma, Spain, 26−30 May 2003, ed. F. Prada, D. Martinez-Delgado, & T. Mahoney, in press [arXiv:astro-ph/0401625]
Cole, A. A. 2001, ApJ, 559, L17
Cole, A. A., Tolstoy, E., Gallagher, J. S., & Smecker-Hane, T. A. 2005, AJ, 129, 1465
Ferraro, F. R., D'Amico, N., Possenti, A., Mignani, R. P., & Paltrinieri, B. 2001, ApJ, 561, 337
Fulbright, J. P., Rich, R. M., & Castro, S. 2004, ApJ, 612, 447
Fuhr, J. R., Martin, G. A., & Wiese, W. L. 1988, J. Phys. Chem. Ref. Data, 17, Suppl. 4 (FMW)
Geisler, D., Smith, V. V., Wallerstein, G., Gonzalez, G., & Charbonnel, C. 2005, AJ, 129, 1428
Girardi, L., Bertelli, G., Bressan, A., et al. 2002, A&A, 391, 195
Gratton, R. G., Carretta, E., Claudi, R., Lucatello, S., & Barbieri, M. 2003, A&A, 404, 187 (G03)
Helmi, A. 2004, MNRAS, 351, 643
Ibata, R. A., Gilmore, G., & Irwin, M. J. 1994, Nature, 370, 194
Ibata, R. A., Gilmore, G., & Irwin, M. J. 1995, MNRAS, 277, 781
Ibata, R. A., Wyse, R. F. G., Gilmore, G., Irwin, M. J., & Suntzeff, N. B. 1997, AJ, 113, 634
Ivans, I. I., Kraft, R. P., Sneden, C., et al. 2001, AJ, 122, 1438
Kravtsov, A. V., Gnedin, O. Y., & Klypin, A. A. 2004, ApJ, 609, 482
Kurucz, R. L. 1993, CD-ROM 13, 18
    http://kurucz.harvard.edu
Layden, A. C., & Sarajedini, A. 2000, AJ, 119, 1760 (LS00)
Lanfranchi, G. A., & Matteucci, F. 2003, MNRAS, 345, 71

Majewski, S. R., Skrutskie, M. F., Weinberg, M. D., & Ostheimer, J. C. 2003, ApJ, 599, 1082

Majewski, S. R., Kunkel, W. E., Law, D. R., et al. 2004, AJ, 128, 245

Marconi, G., Matteucci, F., & Tosi, M. 1994, MNRAS, 270, 35

Marconi, G., Buonanno, R., Castellani, M., et al. 1998, A&A, 330, 453

Martin, G. A., Fuhr, J. R., & Wiese, W. L. 1988, J. Phys. Chem. Ref. Data, 17, Suppl. 3 (MFW)

Mayer, L., Governato, F., Colpi, M., et al. 2001, ApJ, 559, 754

Mateo, M., Udalski, A., Szymansky, M., et al. 1995, AJ, 110, 1141

McWilliam, A. 1997, ARA&A, 35, 503

Mc William, A., & Smecker-Hane, T. 2004, ASP Conf. on Cosmic Abundances as Records of Stellar Evolution and Nucleosynthesis, 2005, ed. F. N. Bash, & T. G. Barnes [arXiv:astro-ph/0409083]

Monaco, L., Ferraro, F. R., Bellazzini, M., & Pancino, E. 2002, ApJ, 578, L47

Monaco, L., Bellazzini, M., Ferraro, F. R., & Pancino, E. 2003, ApJ, 597, L25

Monaco, L., Bellazzini, M., Ferraro, F. R., & Pancino, E. 2004, MNRAS, 353, 874

Monaco, L., Bellazzini, M., Ferraro, F. R., & Pancino, E. 2005, MNRAS, 356, 1396

O'Brian, T. R., Wickliffe, M. E., Lawler, J. E., Whaling, J. W., & Brault, W. 1991, Opt. Soc. Am. J. B Opt. Phys., 8, 1185 (O)

Pasquini, L., Avila, G., Allaert, E., et al. 2000, Proc. SPIE, 4008, 129

Robertson, B., Bullock, J. S., Font, A. S., Johnston, K. V., & Hernquist, L. 2005, ApJ, submitted [arXiv:astro-ph/0501398]

Robin, A. C., Reylé, C., Derrière, S., & Picaud, S. 2003, A&A, 409, 523

Salaris, M., Chieffi, A., & Straniero, O. 1993, ApJ, 414, 580

Schlegel, D. J., Finkbeiner, D. P., & Davis, M. 1998, ApJ, 500, 525

Selvelli, P. L., & Bonifacio, P. 2000, A&A, 364, L1

Shetrone, M. D., Bolte, M., & Stetson, P. B. 1998, AJ, 115, 1888

Shetrone, M. D., Côté, P., & Sargent, W. L. W. 2001, ApJ, 548, 592

Shetrone, M., Venn, K. A., Tolstoy, E., et al. 2003, AJ, 125, 684

Smecker-Hane, T., & Mc William, A. 1999, ASP Conf. Ser., 192, 150

Smecker-Hane, T. A., & McWilliam, A. 2002, ApJ, submitted [arXiv:astro-ph/0205411]

Smith, G., & Raggett, D. S. J. 1981, Journal of Physics B Atomic Molecular Physics, 14, 4015 (SR)

Tolstoy, E., Venn, K. A., Shetrone, M., et al. 2003, AJ, 125, 707

Tolstoy, E., Irwin, M. J., Helmi, A., et al. 2004, ApJ, 617, L119

Trager, S. C., King, I. R., & Djorgovski, S. 1995, AJ, 109, 218

Valenti, J. A., Piskunov, N., & Johns-Krull, C. M. 1998, ApJ, 498, 851

Venn, K. A., Irwin, M., Shetrone, M. D., et al. 2004, AJ, 128, 1177

White, S. D. M., & Rees, M. J. 1978, MNRAS, 183, 341

Wiese, W. L., Smith, M. W., & Miles, B. M. 1969, NSRDS-NBS 22 (NBS)

Wolnik, S. J., Berthel, R. O., & Wares, G. W. 1971, ApJ, 166, L31 (WBW2)

Zaggia, S., Bonifacio, P., Bellazini, M., et al. 2004, Mem. Soc. Astron. It. Suppl., 5, 291

Zaritsky, D., & Harris, J. 2004, ApJ, 604, 167

Online Material

Appendix A: Individual line data

The following tables report the line list and adopted atomic parameters for the program stars. The measured equivalent width and the corresponding abundance obtained for each line are also reported.

Table A.1. Line list and adopted atomic parameters for the program stars. The measured equivalent width and the corresponding abundance obtained for each line are also reported.

Ion	λ (nm)	log gf	Source of log gf (see notes)	EW (pm) 2 300 127	ε	EW (pm) 2 300 196	ε	EW (pm) 2 300 215	ε	EW (pm) 2 409 744	ε	EW (pm) 3 600 073*	ε
Fe I	585.5076	−1.76	FMW	–	–	5.89	7.375	–	–	4.42	7.253	4.44	7.149
Fe I	588.3817	−1.36	FMW	9.19	6.607	10.70	6.763	11.67	7.195	–	–	10.66	6.861
Fe I	595.2718	−1.44	FMW	6.51	6.269	9.42	6.684	–	–	–	–	7.29	6.398
Fe I	602.4058	−0.12	FMW	11.52	6.654	15.93	7.153	13.97	7.173	14.75	7.367	11.14	6.569
Fe I	602.7051	−1.21	FMW	12.20	7.15	14.34	7.335	11.75	7.214	–	–	9.30	6.637
Fe I	605.6005	−0.46	FMW	8.91	6.825	9.66	6.808	9.65	7.031	–	–	7.34	6.535
Fe I	609.6664	−1.93	FMW	5.98	6.666	–	–	9.26	7.352	–	–	6.18	6.702
Fe I	615.1617	−3.30	FMW	15.14	6.671	17.38	6.982	17.52	7.339	16.63	7.263	15.05	6.701
Fe I	616.5360	−1.55	FMW	7.46	6.772	9.78	7.066	9.20	7.19	8.86	7.172	6.80	6.657
Fe I	618.7989	−1.72	FMW	8.18	6.755	10.88	7.108	9.67	7.149	10.19	7.291	9.04	6.895
Fe I	622.6734	−2.22	FMW	2.34	6.116	7.57	7.045	7.73	7.229	7.63	7.238	5.37	6.706
Fe I	651.8366	−2.75	FMW	13.18	6.811	14.61	6.979	17.20	7.677	13.50	7.162	13.83	6.937
Fe I	659.7559	−1.07	FMW	5.97	7.017	6.07	6.968	7.34	7.32	6.72	7.248	4.54	6.747
Fe I	670.3566	−3.16	FMW	11.49	6.823	13.50	7.107	14.97	7.632	12.19	7.225	11.57	6.856
Fe I	673.9521	−4.95	FMW	11.75	6.714	11.36	6.785	–	–	–	–	9.83	6.486
Fe I	674.6954	−4.35	FMW	–	–	6.23	7.124	–	–	6.66	7.284	5.01	6.843
Fe I	679.3258	−2.47	FMW	2.41	6.658	–	–	4.19	7.151	–	–	2.73	6.742
Mg I	552.8405	−0.522	G03	23.92	6.67	25.91	6.811	24.36	6.827	–	–	20.64	6.485
Mg I	571.1088	−1.729	G03	14.75	6.98	16.63	7.125	16.58	7.326	14.16	7.052	12.13	6.612
Mg I	631.8717	−1.945	G03	–	–	7.78	7.279	5.24	7.012	–	–	4.74	6.868
Mg I	631.9237	−2.165	G03	–	–	3.67	6.913	3.73	6.981	4.49	7.12	2.68	6.709
Ca I	585.7451	0.240	SR	19.82	5.381	23.93	5.848	21.37	5.782	20.52	5.719	17.66	5.192
Ca I	586.7562	−1.490	G03	6.94	5.263	8.57	5.643	12.08	6.253	9.27	5.811	6.25	5.231
Ca I	612.2217	−0.315	SR	30.67	5.327	30.52	5.576	41.66	6.086	–	–	26.93	5.298
Ca I	616.9042	−0.797	SR	17.36	5.494	19.67	5.846	19.24	6.089	17.68	5.908	14.76	5.151
Ca I	643.9075	0.390	SR	26.02	5.338	29.40	5.736	28.96	5.854	28.92	5.861	24.25	5.322
Ca I	645.5558	−1.290	SR	14.86	5.535	15.11	5.632	14.67	5.795	13.82	5.687	13.84	5.439
Ca I	649.3781	−0.109	SR	21.22	5.289	21.69	5.351	22.97	5.812	22.43	5.795	18.13	4.933
Ca I	649.9650	−0.818	SR	16.09	5.243	20.09	5.843	21.65	6.364	18.07	5.908	16.61	5.4
Ca I	650.8850	−2.110	NBS	7.53	5.276	7.99	5.550	9.06	5.744	9.75	5.836	5.49	5.082
Ti I	588.0269	−2.045	MFW	13.16	4.002	14.99	4.512	16.08	4.985	14.31	4.684	9.68	3.591
Ti I	590.3315	−2.145	MFW	12.61	4.029	16.09	4.789	12.98	4.544	13.38	4.624	10.91	3.884
Ti I	593.7809	−1.890	MFW	13.52	3.903	15.31	4.403	15.86	4.761	15.38	4.705	13.95	4.088
Ti I	595.3160	−0.329	MFW	15.25	4.023	17.71	4.516	17.94	4.935	17.02	4.826	11.69	3.516
Ti I	597.8541	−0.496	MFW	14.21	3.981	15.55	4.325	17.77	5.039	15.03	4.567	12.59	3.8
Ti I	601.6995	−3.630	MFW	–	–	3.21	4.615	4.47	4.783	3.78	4.611	1.69	3.956
Ti I	606.4626	−1.944	MFW	–	–	13.98	4.219	16.58	4.896	16.49	4.925	13.91	4.08
Ti I	609.1171	−0.423	MFW	11.49	4.081	13.57	4.553	16.34	5.236	12.30	4.571	10.83	4.063
Ti I	609.2792	−1.379	MFW	7.80	3.89	10.40	4.511	8.53	4.35	9.65	4.487	7.01	3.89

Table A.1. continued.

Ion	λ (nm)	log *gf*	Source of log *gf* (see notes)	EW (pm) 3 600 230	ϵ	EW (pm) 3 600 262	ϵ	EW (pm) 3 600 302	ϵ	EW (pm) 3 700 178*	ϵ	EW (pm) 3 800 199	ϵ
Fe I	585.5076	−1.76	FMW	6.73	7.701	–	–	–	–	4.42	7.217	3.06	6.832
Fe I	588.3817	−1.36	FMW	11.04	7.257	9.78	6.87	8.95	6.902	12.59	7.134	8.77	6.514
Fe I	595.2718	−1.44	FMW	10.48	7.249	9.60	6.952	10.97	7.428	–	–	7.28	6.376
Fe I	602.4058	−0.12	FMW	14.35	7.397	14.91	7.335	11.72	7.037	12.74	6.777	9.52	6.18
Fe I	602.7051	−1.21	FMW	10.62	7.166	10.34	6.98	9.77	7.077	11.18	6.929	7.11	6.235
Fe I	605.6005	−0.46	FMW	–	–	–	–	9.99	7.307	9.79	6.939	5.76	6.147
Fe I	609.6664	−1.93	FMW	9.35	7.493	7.49	7.071	8.41	7.388	8.95	7.174	4.23	6.378
Fe I	615.1617	−3.30	FMW	15.16	7.221	15.05	6.991	14.02	7.062	18.70	7.176	11.90	6.428
Fe I	616.5360	−1.55	FMW	9.38	7.341	7.81	6.974	–	–	9.53	7.114	5.69	6.435
Fe I	618.7989	−1.72	FMW	10.02	7.352	10.75	7.36	8.67	7.163	9.35	6.959	6.20	6.415
Fe I	622.6734	−2.22	FMW	7.26	7.221	8.91	7.448	8.27	7.492	5.19	6.761	3.07	6.321
Fe I	651.8366	−2.75	FMW	15.48	7.638	13.44	7.125	13.62	7.39	13.99	6.929	10.83	6.586
Fe I	659.7559	−1.07	FMW	6.60	7.23	5.85	7.087	5.13	7.053	7.75	7.328	2.73	6.284
Fe I	670.3566	−3.16	FMW	10.61	7.083	12.58	7.271	11.40	7.282	15.48	7.423	8.72	6.555
Fe I	673.9521	−4.95	FMW	12.39	7.381	10.84	6.947	9.69	6.914	11.79	6.816	7.40	6.47
Fe I	674.6954	−4.35	FMW	5.59	7.18	7.14	7.384	5.87	7.262	5.65	7.053	–	–
Fe I	679.3258	−2.47	FMW	6.63	7.608	4.56	7.238	4.00	7.196	4.92	7.243	–	–
Mg I	552.8405	−0.522	G03	26.90	7.019	–	–	26.42	7.003	25.88	6.831	20.68	6.617
Mg I	571.1088	−1.729	G03	16.13	7.383	14.74	7.102	13.29	7.044	12.35	6.621	10.03	6.425
Mg I	631.8717	−1.945	G03	5.97	7.137	7.10	7.309	3.88	6.841	5.53	7.042	2.45	6.475
Mg I	631.9237	−2.165	G03	6.41	7.428	6.33	7.413	4.91	7.246	–	–	1.96	6.575
Ca I	585.7451	0.240	SR	19.10	5.772	17.91	5.4	20.24	5.78	18.14	5.09	15.44	5.501
Ca I	586.7562	−1.490	G03	7.53	5.712	9.25	5.814	9.00	5.859	10.79	5.788	3.81	5.442
Ca I	612.2217	−0.315	SR	30.57	5.856	26.93	5.432	31.74	5.737	41.80	5.91	24.84	5.805
Ca I	616.9042	−0.797	SR	16.63	6.011	17.27	5.785	17.26	6.016	20.98	5.916	13.52	5.657
Ca I	643.9075	0.390	SR	24.07	5.723	23.66	5.415	28.40	5.894	27.02	5.399	21.83	5.641
Ca I	645.5558	−1.290	SR	14.45	6.063	15.14	5.88	13.90	5.875	14.39	5.392	10.05	5.564
Ca I	649.3781	−0.109	SR	20.98	5.653	19.90	5.418	20.23	5.679	20.86	5.125	18.14	5.604
Ca I	649.9650	−0.818	SR	16.19	5.876	16.61	5.629	17.58	6.019	15.73	5.102	13.18	5.564
Ca I	650.8850	−2.110	NBS	7.32	5.657	6.72	5.43	8.86	5.79	9.14	5.527	–	–
Ti I	588.0269	−2.045	MFW	12.47	4.671	11.71	4.235	11.48	4.349	13.54	4.106	8.06	4.387
Ti I	590.3315	−2.145	MFW	11.11	4.527	11.98	4.395	10.54	4.285	13.31	4.192	7.33	4.412
Ti I	593.7809	−1.890	MFW	13.78	4.754	12.89	4.274	14.18	4.709	14.58	4.102	8.04	4.24
Ti I	595.3160	−0.329	MFW	15.62	4.902	13.83	4.184	13.32	4.318	12.88	3.629	11.25	4.335
Ti I	597.8541	−0.496	MFW	13.19	4.531	12.35	4.068	14.25	4.649	15.84	4.209	8.98	4.144
Ti I	601.6995	−3.630	MFW	3.09	4.703	3.59	4.661	2.81	4.48	3.24	4.382	–	–
Ti I	606.4626	−1.944	MFW	13.25	4.655	14.44	4.532	13.73	4.628	14.89	4.147	10.04	4.502
Ti I	609.1171	−0.423	MFW	10.83	4.578	11.86	4.5	12.48	4.783	14.67	4.556	6.40	4.262
Ti I	609.2792	−1.379	MFW	7.39	4.374	7.72	4.253	9.62	4.606	8.87	4.141	3.56	4.275

Table A.1. continued.

Ion	λ (nm)	log *gf*	Source of log *gf* (see notes)	EW (pm) 3 800 204	ε	EW (pm) 3 800 318	ε	EW (pm) 3 800 319	ε	EW (pm) 3 800 336*	ε
Fe I	585.5076	–1.76	FMW	–	–	4.61	7.241	–	–	–	–
Fe I	588.3817	–1.36	FMW	7.89	6.138	9.56	6.771	–	–	8.71	6.641
Fe I	595.2718	–1.44	FMW	5.21	5.89	8.47	6.692	–	–	8.23	6.675
Fe I	602.4058	–0.12	FMW	9.69	5.95	14.80	7.274	–	–	12.01	6.835
Fe I	602.7051	–1.21	FMW	5.84	5.867	9.99	6.858	–	–	10.99	7.049
Fe I	605.6005	–0.46	FMW	5.00	5.896	9.71	7.008	–	–	7.55	6.689
Fe I	609.6664	–1.93	FMW	12.91	6.007	7.39	6.993	–	–	7.17	6.986
Fe I	615.1617	–3.30	FMW	1.13	5.933	15.52	6.987	–	–	16.32	7.04
Fe I	616.5360	–1.55	FMW	4.00	6.027	7.74	6.9	–	–	7.25	6.853
Fe I	618.7989	–1.72	FMW	4.86	6.05	9.24	7.033	–	–	7.53	6.771
Fe I	622.6734	–2.22	FMW	2.25	6.014	7.37	7.128	–	–	7.11	7.112
Fe I	651.8366	–2.75	FMW	9.51	6.086	12.81	6.947	–	–	12.48	6.862
Fe I	659.7559	–1.07	FMW	–	–	5.63	6.994	–	–	5.52	7.041
Fe I	670.3566	–3.16	FMW	6.42	6.005	11.91	7.083	–	–	–	–
Fe I	673.9521	–4.95	FMW	5.76	5.998	9.47	6.648	–	–	10.34	6.71
Fe I	674.6954	–4.35	FMW	–	–	5.72	7.096	–	–	5.85	7.103
Fe I	679.3258	–2.47	FMW	–	–	–	–	–	–	–	–
Mg I	552.8405	–0.522	G03	19.95	6.239	25.04	6.858	18.45	6.469	24.82	6.866
Mg I	571.1088	–1.729	G03	10.90	6.313	14.70	7.06	10.81	6.653	14.66	7.101
Mg I	631.8717	–1.945	G03	–	–	3.54	6.702	–	–	–	–
Mg I	631.9237	–2.165	G03	–	–	2.38	6.681	–	–	4.07	7.067
Ca I	585.7451	0.240	SR	14.48	4.969	23.54	5.949	13.20	5.347	21.15	5.654
Ca I	586.7562	–1.490	G03	–	–	12.35	6.278	–	–	9.14	5.667
Ca I	612.2217	–0.315	SR	–	–	29.75	5.621	18.71	5.267	–	–
Ca I	616.9042	–0.797	SR	11.15	4.938	17.28	5.77	9.69	5.237	16.82	5.6
Ca I	643.9075	0.390	SR	–	–	28.72	5.848	17.55	5.28	25.90	5.529
Ca I	645.5558	–1.290	SR	8.64	5.092	14.54	5.749	7.43	5.356	14.79	5.691
Ca I	649.3781	–0.109	SR	16.22	4.873	23.18	5.826	15.61	5.477	22.53	5.658
Ca I	649.9650	–0.818	SR	11.42	4.958	19.68	6.077	12.49	5.687	18.59	5.828
Ca I	650.8850	–2.110	NBS	–	–	9.91	5.841	–	–	7.59	5.389
Ti I	588.0269	–2.045	MFW	3.97	3.56	15.47	4.822	3.66	4.069	14.00	4.405
Ti I	590.3315	–2.145	MFW	4.44	3.744	12.62	4.436	3.67	4.187	12.11	4.19
Ti I	593.7809	–1.890	MFW	4.94	3.55	15.34	4.621	4.30	4.029	14.55	4.336
Ti I	595.3160	–0.329	MFW	8.42	3.599	17.81	4.875	6.63	3.917	16.24	4.463
Ti I	597.8541	–0.496	MFW	6.43	3.515	16.98	4.849	7.17	4.14	14.47	4.261
Ti I	601.6995	–3.630	MFW	–	–	3.94	4.657	–	–	4.33	4.521
Ti I	606.4626	–1.944	MFW	6.83	3.78	16.48	4.829	6.06	4.293	16.14	4.627
Ti I	609.1171	–0.423	MFW	4.41	3.744	13.42	4.706	5.51	4.346	13.62	4.626
Ti I	609.2792	–1.379	MFW	1.94	3.711	9.20	4.403	–	–	8.93	4.214

Table A.1. continued.

Ion	λ (nm)	log *gf*	Source of log *gf* (see notes)	EW (pm) 4 207 953*	ε	EW (pm) 4 303 773	ε	EW (pm) 4 304 445	ε	EW (pm) 4 402 285	ε	EW (pm) 4 408 968	ε
Fe I	585.5076	−1.76	FMW	5.63	7.408	3.06	6.896	4.90	7.28	4.63	7.275	5.11	7.309
Fe I	588.3817	−1.36	FMW	11.23	7.057	10.20	6.836	11.99	7.326	–	–	12.23	7.2
Fe I	595.2718	−1.44	FMW	–	–	8.60	6.666	–	–	9.46	7.076	8.97	6.75
Fe I	602.4058	−0.12	FMW	12.90	6.953	13.07	6.936	13.48	7.139	13.24	7.238	14.22	7.087
Fe I	602.7051	−1.21	FMW	11.81	7.169	–	–	11.50	7.219	10.76	7.235	10.57	6.91
Fe I	605.6005	−0.46	FMW	8.70	6.822	8.52	6.741	9.16	6.936	–	–	10.45	7.048
Fe I	609.6664	−1.93	FMW	7.32	6.959	6.15	6.739	8.17	7.164	7.72	7.191	8.38	7.137
Fe I	615.1617	−3.30	FMW	16.99	7.166	14.48	6.781	13.99	6.905	13.75	7.143	16.13	7.114
Fe I	616.5360	−1.55	FMW	8.92	7.082	5.83	6.531	8.76	7.113	9.79	7.447	9.19	7.105
Fe I	618.7989	−1.72	FMW	9.47	7.052	7.88	6.751	10.19	7.27	9.90	7.366	9.18	6.993
Fe I	622.6734	−2.22	FMW	8.24	7.249	4.73	6.647	7.65	7.205	6.40	7.078	6.36	6.966
Fe I	651.8366	−2.75	FMW	14.04	7.11	11.96	6.765	14.87	7.422	12.52	7.254	15.48	7.373
Fe I	659.7559	−1.07	FMW	6.24	7.087	–	–	7.29	7.264	7.17	7.293	6.75	7.126
Fe I	670.3566	−3.16	FMW	12.82	7.193	11.45	6.965	11.33	7.101	10.31	7.13	11.01	6.972
Fe I	673.9521	−4.95	FMW	–	–	9.24	6.586	10.66	6.97	9.42	7.021	10.28	6.888
Fe I	674.6954	−4.35	FMW	5.90	7.078	–	–	6.41	7.25	4.36	7.058	6.19	7.253
Fe I	679.3258	−2.47	FMW	4.09	7.068	4.42	7.103	3.60	6.988	5.86	7.463	5.15	7.278
Mg I	552.8405	−0.522	G03	26.88	6.953	21.07	6.563	–	–	24.18	6.949	23.99	6.79
Mg I	571.1088	−1.729	G03	13.37	6.858	13.48	6.856	15.72	7.268	13.61	7.108	12.82	6.774
Mg I	631.8717	−1.945	G03	6.26	7.135	2.48	6.456	6.43	7.161	7.58	7.389	–	–
Mg I	631.9237	−2.165	G03	3.64	6.927	2.94	6.775	–	–	3.80	6.995	3.20	6.862
Ca I	585.7451	0.240	SR	17.97	5.36	20.31	5.702	19.18	5.761	18.74	5.982	20.40	5.784
Ca I	586.7562	−1.490	G03	8.13	5.588	6.72	5.47	7.18	5.663	6.97	5.865	8.81	5.888
Ca I	612.2217	−0.315	SR	34.59	5.836	27.12	5.529	28.52	5.794	24.80	5.827	30.80	5.847
Ca I	616.9042	−0.797	SR	19.00	6.02	16.17	5.619	17.49	6.103	18.10	6.549	17.85	5.96
Ca I	643.9075	0.390	SR	26.92	5.7	23.20	5.406	23.37	5.637	24.34	6.013	25.33	5.678
Ca I	645.5558	−1.290	SR	13.85	5.593	10.57	5.163	14.76	6.059	13.22	6.149	14.53	5.887
Ca I	649.3781	−0.109	SR	20.17	5.405	19.33	5.347	20.40	5.755	17.64	5.704	21.24	5.675
Ca I	649.9650	−0.818	SR	17.16	5.648	16.77	5.655	15.94	5.77	15.75	6.106	18.30	5.97
Ca I	650.8850	−2.110	NBS	8.22	5.556	5.68	5.307	5.06	5.34	5.71	5.677	7.25	5.676
Ti I	588.0269	−2.045	MFW	16.14	4.879	10.28	4.003	11.33	4.419	9.77	4.594	11.74	4.461
Ti I	590.3315	−2.145	MFW	13.87	4.574	8.84	3.92	10.86	4.457	10.49	4.837	12.52	4.692
Ti I	593.7809	−1.890	MFW	14.79	4.453	10.84	3.938	11.13	4.231	11.23	4.7	13.69	4.597
Ti I	595.3160	−0.329	MFW	16.82	4.627	12.91	4.008	15.24	4.731	14.01	4.95	14.05	4.368
Ti I	597.8541	−0.496	MFW	14.40	4.309	11.65	3.942	13.06	4.444	12.22	4.722	13.10	4.357
Ti I	601.6995	−3.630	MFW	3.52	4.51	–	–	1.70	4.429	1.85	4.818	1.95	4.63
Ti I	606.4626	−1.944	MFW	–	–	–	–	12.78	4.513	12.89	5.011	14.13	4.665
Ti I	609.1171	−0.423	MFW	12.29	4.462	8.95	4.05	10.64	4.515	10.41	4.853	11.87	4.662
Ti I	609.2792	−1.379	MFW	8.93	4.3	5.96	4.024	6.83	4.306	6.76	4.63	8.42	4.568

* Star showing TiO molecular bands in the spectra.

FMW – Fuhr et al. (1988); G03 – Gratton et al. (2003); SR – Smith et al. (1981); NBS – Wiese et al. (1969); MFW – Martin et al. (1988).

Table A.2. Iron line list and adopted atomic parameters for star #3800319. The measured equivalent width and the corresponding abundance obtained for each line are also reported.

Ion	λ (nm)	log gf	Source of log gf (see notes)	EW (pm) 3 800 319	ϵ
Fe I	487.1318	−0.410	FMW	17.32	5.949
Fe I	491.8994	−0.370	FMW	17.84	5.958
Fe I	492.0502	0.060	FMW	30.56	6.368
Fe I	495.7298	−0.342	WBW2	17.69	5.878
Fe I	495.7596	0.127	WBW2	28.12	6.162
Fe I	500.6119	−0.615	FMW	22.38	6.571
Fe I	501.2068	−2.642	FMW	23.42	6.398
Fe I	505.1635	−2.795	FMW	22.54	6.528
Fe I	511.0413	−3.760	FMW	18.78	5.715
Fe I	517.1596	−1.793	FMW	20.64	6.045
Fe I	519.1454	−0.551	O	18.57	6.362
Fe I	519.2344	−0.421	O	14.89	5.643
Fe I	519.4941	−2.090	FMW	18.75	6.144
Fe I	522.7189	−1.228	O	23.52	5.867
Fe I	523.2940	−0.190	FMW	19.94	6.012
Fe I	526.6555	−0.490	FMW	19.96	6.379
Fe I	527.0356	−1.510	FMW	25.96	6.378
Fe I	532.4179	−0.240	FMW	17.49	6.123
Fe I	532.8039	−1.466	FMW	43.04	6.118
Fe I	532.8531	−1.850	O	22.24	6.302
Fe I	537.1489	−1.645	FMW	29.90	5.86
Fe I	539.7128	−1.993	FMW	26.15	5.884
Fe I	540.5775	−1.844	FMW	26.33	5.852
Fe I	542.9696	−1.879	FMW	32.89	6.209
Fe I	543.4524	−2.122	FMW	22.59	5.806
Fe I	544.6916	−1.930	FMW	28.62	6.095
Fe I	545.5609	−2.091	O	36.09	6.604
Fe I	561.5644	−0.140	FMW	19.44	6.333
Fe I	595.2718	−1.440	FMW	5.11	6.135
Fe I	602.7051	−1.210	FMW	6.22	6.195
Fe I	616.5360	−1.550	FMW	5.95	6.57
Fe I	670.3566	−3.160	FMW	4.69	6.127

FMW – Fuhr et al. (1988); WBW2 – Wolniket et al. (1971); O – O'Brian et al. (1991).